Sensitivity of voxel-based estimations of leaf area density with terrestrial LiDAR to vegetation structure and sampling limitations: A simulation experiment

Maxime Soma, François Pimont, Jean-Luc Dupuy

To cite this version:

Maxime Soma, François Pimont, Jean-Luc Dupuy. Sensitivity of voxel-based estimations of leaf area density with terrestrial LiDAR to vegetation structure and sampling limitations: A simulation experiment. Remote Sensing of Environment, 2021, 257, pp.112354. 10.1016/j.rse.2021.112354 . hal-03353461

HAL Id: hal-03353461
https://hal.inrae.fr/hal-03353461

Submitted on 9 Mar 2023

Version of Record: https://www.sciencedirect.com/science/article/pii/S0034425721000729
Manuscript_5cc37742333beaa0f138d1a4e4253ee4

Sensitivity of voxel-based estimations of Leaf Area Density with Terrestrial LiDAR to vegetation structure and sampling limitations: a simulation experiment

Maxime Soma[1,2*], François Pimont[1], Jean-Luc Dupuy[1]

[1] UR 629 Ecologie des Forêts Méditerranéennes (URFM), INRAe, 84914 Avignon, France

[2] UMR 114 EMMAH, UMT CAPTE, INRAe, 84914 Avignon, France

Abstract

The need for fine scale description of vegetation structure is increasing as Leaf Area Density (LAD, m^2/m^3) becomes a critical parameter to understand ecosystem functioning and energy and mass fluxes in heterogeneous ecosystems. Terrestrial Laser Scanning (TLS) has shown great potential for retrieving the foliage area at stand, plant or voxel scales. Several sources of measurement errors have been identified and corrected over the past years. However, measurements remain sensitive to several factors, including, 1) voxel size and vegetation structure within voxels, 2) heterogeneity in sampling from TLS instrument (occlusion and shooting pattern), the consequences of which have been seldom analyzed at the scale of forest plots. In the present paper, we aimed at disentangling biases and errors in plot-scale measurements of LAD with TLS in a simulated vegetation scene. Two negative biases were formerly attributed to (i) the unsampled voxels and to (ii) the subgrid vegetation heterogeneity (i.e. clumping effect), and then quantified, thanks to a the simulation experiment providing known LAD references at voxel scale, vegetation manipulations and unbiased point estimators. We used confidence intervals to evaluate voxel-scale measurement accuracy.

We found that the unsampled voxel effect (i) led to underestimations with the “mean layer” method –commonly used to fill unsampled voxels- for small voxels (0.1-0.2 m) and/or low number of scans (<4). It was explained by the spatial correlations in vegetation, which induced that dense voxels were more often occluded by dense neighbors than light voxels. The distribution of the bias was heterogeneous in canopy, the bias being stronger at mid canopy where occlusion started, but smaller in highly-occluded upper layers. This somehow counterintuitive result was explained by a more random sampling of upper layers, but could highly depend on vegetation structure.

The subgrid vegetation heterogeneity effect (ii) was confirmed to increase with voxel size, yet, the magnitude of this bias -quantified with vegetation manipulation- was found to be more homogeneously-distributed than the unsampled voxel effect.

Overall, we found that no scenario was unbiased. However, an intermediate voxel size (0.5m) was the best option, because the relatively homogeneous subgrid effect could be handled with a single correction factor and voxel-scale measurements errors were reasonable. On the contrary, smaller voxels led to poor voxel-scale measurements and variable biases in magnitude and spatial distribution with sampling design. However, more similar research in other context is required to adapt these conclusions to other forest plots.

Keywords: Terrestrial LiDAR; Leaf Area Density (LAD); LAI; Occlusion; Voxel

1. Introduction

The tridimensional distribution of vegetation in forest ecosystems constitutes a complex surface of exchange between canopies, ground and atmosphere, driving mass and energy fluxes (Norman and Campbell, 1989). Characterizing its structure is key for monitoring health and carbon storage of forests, but also for understanding and modelling tree ecophysiological processes. This amount of vegetation can be described by the Leaf Area Density (LAD) distribution, i.e. the total leaf area per unit of volume (Weiss et al., 2004). In the past decade, LiDAR technologies have been used for measuring LAD at various scales. Airborne LiDAR can provide canopy profile estimates at coarse grains and over large areas, which is very useful for forests monitoring, but estimates can hardly be evaluated against ground references (Kamoske et al., 2019; Stark et al., 2012). Meanwhile, Terrestrial laser scanning (TLS) has been used successfully for local measuring, such as the total leaf area of individual trees (Béland et al., 2011; Hosoi et al., 2010; Hu et al., 2018) and the LAD profiles at plot scale (Pimont et al., 2016; Schneider et al., 2019). The detailed 3D point clouds provided by TLS can closely describe the scene in three dimensions, the density of points being related to the presence of vegetation (Durrieu et al., 2008). LAD or PAD (Plant Area Density, i.e. vegetation area density, indiscriminate between leaf and wood material) has been estimated from a variety of methods based on the similar theoretical background related to the attenuation of light in uniform medium. Typically, most commonly used methods are inherited from Leaf Area Index measurements, and are based on the Beer's law theory (Yan et al., 2019), i.e. the exponential attenuation of the transmittance along the path of the beam, which readily relates the gap fraction and the attenuation coefficient of the medium. Path length distribution models fully exploit the 3D information contained in point clouds by accounting for the path length of beam within canopy before its interception, which has been shown to provide better estimates (Yan et al., 2019), whether integrated to Beer's law approaches (Zhao et al., 2015) or directly arising from contact frequency method (Béland et al., 2011; Pimont et al., 2019, 2018). LAD estimates can be retrieved either for a given layer in order to yield LAD profiles (Hosoi and Omasa, 2006; Zhao et al., 2015) or directly within each voxel (Béland et al., 2011; Soma et al., 2018). Measuring LAD at voxel scale is particularly relevant for optical measurements in non-uniform canopies context because it allows to discriminate gaps and within crown volumes, thus limiting clumping effect (Yan et al., 2019). Pimont et al. (2018) provided a detailed comparison of voxel-based methods for the estimation of the attenuation coefficient within a single voxel, which is linearly related to LAD/PAD. They introduced a more straightforward approach based on Maximum Likelihood Estimation (MLE) and suggested corrections when the beam number was low and the vegetation element size was not very small with respect to voxel size, resulting in an unbiased estimator. In general, most theoretical estimates compare reasonably well with reference measurements (Bailey and Mahaffee, 2017; Béland et al., 2011; Hu et al., 2018; Pimont et al., 2016; Soma et al., 2018). However, TLS-based estimations are also affected by several biases, arising both from inversion method and instrument limitations (Yan et al., 2019).

With the voxel-based approach, LiDAR estimates of LAD/PAD generally decrease with voxel size (Bailey and Mahaffee, 2017; Béland et al., 2014a; Soma et al., 2018). Although the effect of voxel size has been repeatedly observed (Cifuentes et al., 2014; Huang and Pretzsch, 2010; Li et al., 2016) , few studies conducted a complete analysis of this effect (Béland et al., 2014a; Grau et al., 2017). Such an effect has been attributed to vegetation clumping, which induces the presence of heterogeneities in the vegetation structure inside the voxel, referred to as subgrid vegetation heterogeneity. The choice of too large voxels regarding vegetation structure hampers a proper discretization of gaps and clumps, leading to a negative bias in estimates as a consequence of Jensen inequality (Ruel and Ayres, 1999). Additionally, for some instruments, some critical overestimations of LAD occur as distance from scanner increases. This bias has been attributed to the increase in effective footprint of the beam associated with beam divergence (Soma et al. 2018). Both effects can be accounted for through an adequate modelling of the LiDAR signal (Béland et al., 2014b, 2011) or simple calibration coefficients (Soma et al. 2018). Such calibrations have been included in the unbiased estimator approach presented in Pimont et al. (2019), in a new formulation of the estimation of the LAD, which also includes a rigorous incorporation of the wood element volume and multiview LiDAR data (Pimont et al. 2019).

Another important TLS drawback at plot scale, is the spatial variation in sampling quality within point clouds (Schneider et al., 2019; Wilkes et al., 2017). Indeed, the geometry of the shooting pattern of most TLS instruments (such as FARO 130X) has a fixed angular step resolution. Hence, the beam density decreases with distance to scanner. The second source of variation in beam sampling is vegetation occlusion: when a beam is fully intercepted (single hit for monoecho TLS or the last return in case of multiecho TLS), it cannot explore beyond the intercepting voxel. This implies that fewer beams remain when vegetation is present between the scanner and the voxel of interest. Both geometry and occlusion contribute to the occurrence of unsampled voxels, where no information or limited information is available. Since the reliability of LAD estimation within a given voxel strongly depends on the number of beams exploring each voxel (Pimont et al., 2018), random errors in individual voxels are very large when beam number is low. Some point estimators are theoretically unbiased (Pimont et al., 2019, 2018), so that one could expect that the random errors will cancel when averaged over a large number of voxels, e.g. when vertical profiles are computed.

This assumption, however, might not be correct in the field because of the presence of unsampled voxels in the context of heterogeneous canopy. Indeed, one could expect that unsampled voxels would mostly be located in dense vegetation spots, where occlusion is the strongest. At plot scale, this could result in a sampling bias, leading to a potential underestimation of the mean LAD. Typically, the most commonly used methods for correcting for occlusion relies on the mean estimate in layers, i.e. on estimates within explored areas, which might not be representative of occluded areas in clumped vegetation context. To date, few studies have conducted an analysis of occlusion distribution, magnitude and mechanisms at tree (Béland et al., 2011; Yun et al., 2019) or plot scale (Morsdorf et al., 2018; Schneider et al., 2019). Moreover, these studies did not formally disentangle the relative contributions of unsampled voxels from subgrid vegetation heterogeneity, since both vary with voxel size. Also, most previous studies carried out at tree or forest-plot scales relied on point estimates with theoretical biases, which complicates the analysis of biases at tree or plot scales.

To improve sampling quality, a widespread practice during data acquisition is to acquire multiple scans across the scene in order to increase both absolute number of beams and variety of viewpoints (Côté et al., 2011; Wilkes et al., 2017). Moreover, the number of scans used in the field and the scanner resolution are generally limited given technical constraints, such as time to proceed or storage capability (Wilkes et al., 2017). This implies some constraints on voxel size used for estimations, since the fraction of non-explored voxels strongly rises as voxel size decreases (Béland et al., 2014a). Scanning design and post-processing recommendations accounting for these sampling limitations are generally dedicated to applications such as detection of stems or measurement of tree geometrical features (e.g. diameter) (Gollob et al., 2019; Wilkes et al., 2017), but recommendations for description of canopies features are still rare at plot scale (Schneider et al., 2019).

Improving our understanding of the impacts of both heterogeneity effect and occlusion relying on actual data is very challenging because of the lack of accuracy in references, particularly in dense and complex canopy structure, while the estimation of leaf projection factor or leaf fraction are additional sources of errors. In this difficult context, a simulation framework is mandatory to provide a perfectly controlled environment to test various configurations and methods of estimations and disentangle multiple sources of biases (Morsdorf et al., 2018; Yan et al., 2019), as done in Grau et al., (2017). In the present study, we rely on numerical experiments to analyze the sensitivity of LAD estimations to biases arising from (1) vegetation heterogeneity and (2) heterogeneity of the sampling quality at plot scale, which depends on both vegetation structure at canopy scale and sampling design. We performed these simulations with unbiased point estimators in the framework of a Mediterranean canopy sampled with a single echo terrestrial LiDAR. Here, we expect to disentangle and better understand the mechanisms affecting estimations in the field, to analyze their magnitude and how they distribute in forest plots, in order to finally derive recommendations on sampling design and selection of appropriate voxel sizes.

2. Numerical experiments

2.1. Overview

The aim of the numerical experiments was to disentangle biases, errors and limitations arising from voxel size and number of scans for the estimation of LAD in heterogeneous vegetation. For this, we first generated a high resolution reference LAD field that had to meet the following requirements: (i) it had to be as representative as possible of natural vegetation, with dense clumps (corresponding to tree crowns) surrounded by empty locations (ii) it should be realistic for a forest plot, in terms of both LAI and LAD profile, as occlusion patterns are highly sensitive to vegetation attenuation coefficient.

Generation of the LAD reference field (LAD_{REF}) is described in section 2.2. This field had a resolution of 0.1 m. An additional smoother reference fields of the same vegetation scene ($\mathrm{LAD}_{\mathrm{REF\ s0.5}}$) was generated by coarsening the resolution to 0.5 m.

Then, we simulated point clouds that would have been produced by a LiDAR scanning on vegetation corresponding to reference LAD fields under different configurations (number and position of scans). Following Soma et al. (2018) and Pimont et al. (2019), the effective attenuation coefficient λ_{eff} in a given voxel, which is the rate at which beam density is attenuated by vegetation from a given scan position, relates to LAD_{REF} as follows:

$$\lambda_{eff} = \frac{G}{FH} LAD_{REF} \tag{1}$$

where G is the leaf projection function, F is the leaf fraction and H is a calibration function which accounts for both voxel size and distance to scanner. To simulate the influence of these factors on LAD estimation, we computed the distribution of effective attenuation coefficient (λ_{eff}) for each scan position, which corresponds to the perception of LAD_{REF} by the instrument. In order to remain representative of typical field conditions, a maximum of 5 scans was performed in a 10 m X 10 m virtual scene. Then for each scan position, the traversal algorithm was applied to the λ_{eff}-3D field to simulate the perceived point clouds, following parameters arising from vegetation and scanner properties (Eq. 1). The details of the point cloud simulations are presented in section 2.3.

Finally, LAD estimates were retrieved from these point clouds with different voxel sizes using a traversal algorithm and calibrations provided by field experiments (Soma et al., 2018). The information from multiple scans was combined using the formulation of Pimont et al., (2019) (section 2.4). The last section 2.5 describes how we analyzed bias and errors in these estimations. A workflow diagram picturing the methodology used in this work is available in Figure 1.

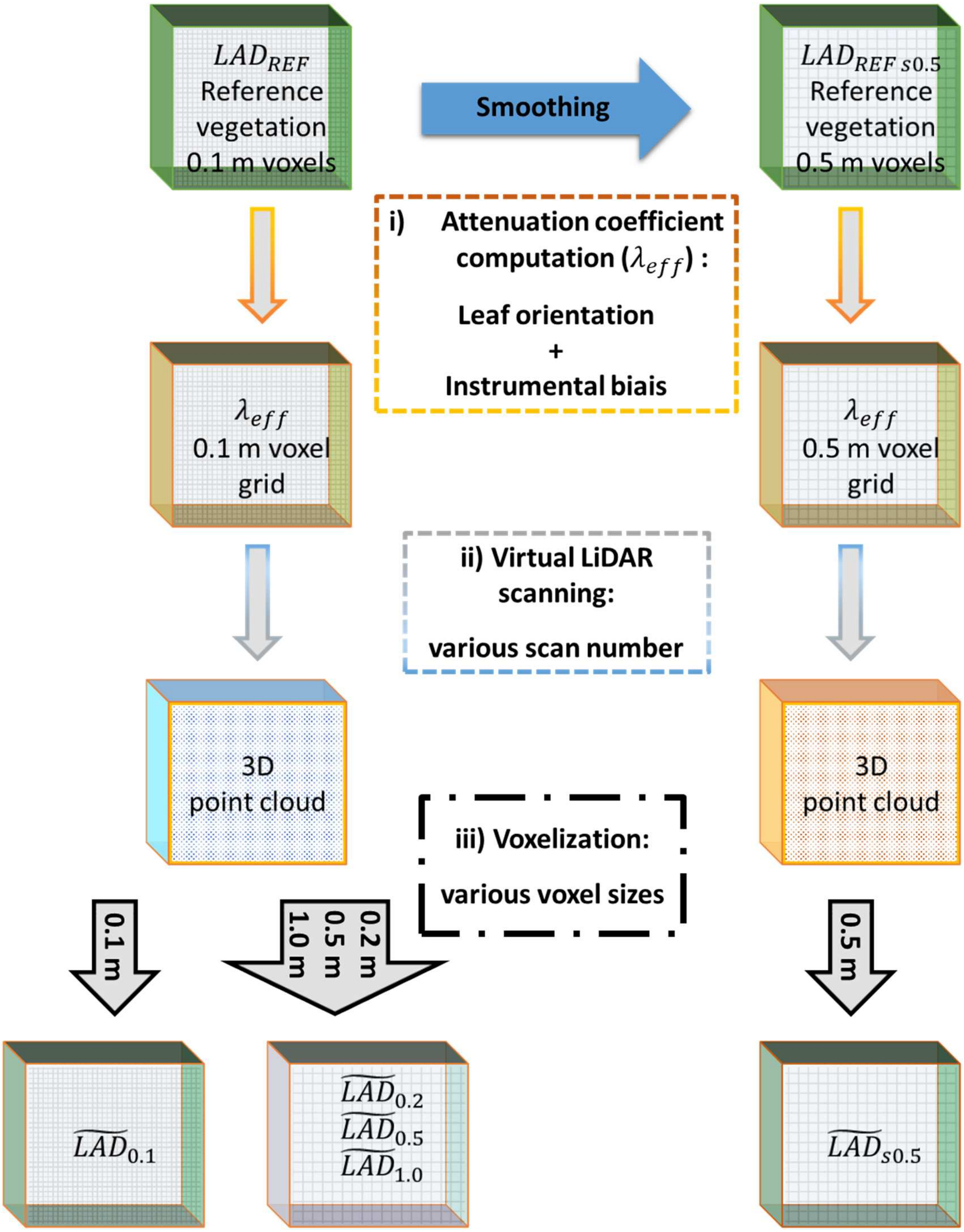

Figure 1. Workflow diagram of simulated LAD scenes and used references. LAD_{REF} is the vegetation reference distribution at 0.1 m heterogeneity scale. $LAD_{REF\,s0.5}$ is the same reference distribution, but at 0.5 m heterogeneity scale. λ_{eff} is the attenuation coefficient. $\widetilde{LAD}$ is the estimated vegetation distribution, with voxel sizes in subscripts.

2.2. Vegetation scene

A 3D virtual vegetation scene described from voxelized LAD_{REF} values was generated from a clumped spatial distribution simulated with *RandomFields* R package (Schlather et al., 2015) in a grid with 0.1 m resolution. The mean clump size, representative of tree crown diameter, was 4 m. This virtual scene was cubic with an extent of 10 m in each grid dimension. The canopy height was thus h=10 m. The voxel size was set to 0.1 m.

The vegetation scene included a realistic vertical profile, with little vegetation below 3 m, an increase to a maximum of LAD values at 7 m, and a decrease until top canopy (see Appendix A). This scene also included random occurrences of 1 m extent local decreases in LAD, with gaps (LAD equals to zero) in 30% of the voxels. This resulted in a vegetation scene with a 70% cover fraction with spatial aggregates corresponding to plant clumps (Figure 2). Such gap distribution was built to analyze the effect of intermediate scale heterogeneity in tree crowns (see spatial correlation in Appendix B). The LAI of the virtual scene was about 3.8, which corresponds to a mean LAD of 0.38 m^{-1} (the scene vertical extent was 10 m). Maximal LAD values reached 3.8 m^{-1}. These vegetation properties match the field measurements of a long-term experimental site characteristic of Mediterranean ecosystems (Simioni et al., 2016). The same scene was formerly used in Soma et al. 2020, to evaluate the effect of a kriging method for unsampled voxels (Soma et al. 2020).

A leaf projection function was implemented to complete vegetation properties following:

$$G(\theta,z)=\frac{1}{2}+0.4\frac{z}{h}\cos(2\theta) \qquad (2)$$

where θ is the angle between the beams and the vertical and ranges between 0 and π. According to this setting leaves are planophile near the canopy top ($z\approx h$), with G=0.9 for vertical beams ($\theta\approx 0$ or $\theta\approx\pi$) and 0.1 for horizontal beams ($\theta\approx\frac{\pi}{2}$), and random near the ground ($z\approx 0$), with G=0.5.

At last, leaf fraction was parameterized to account for fine woody material and leaf association along vertical axis following:

$$F(z)=\left(0.1+0.8\frac{z}{h}\right)^2 \qquad (3)$$

Leaf fraction was hence 0.9 at canopy top ($z\approx h$) and 0.1 near the ground ($z\approx 0$).

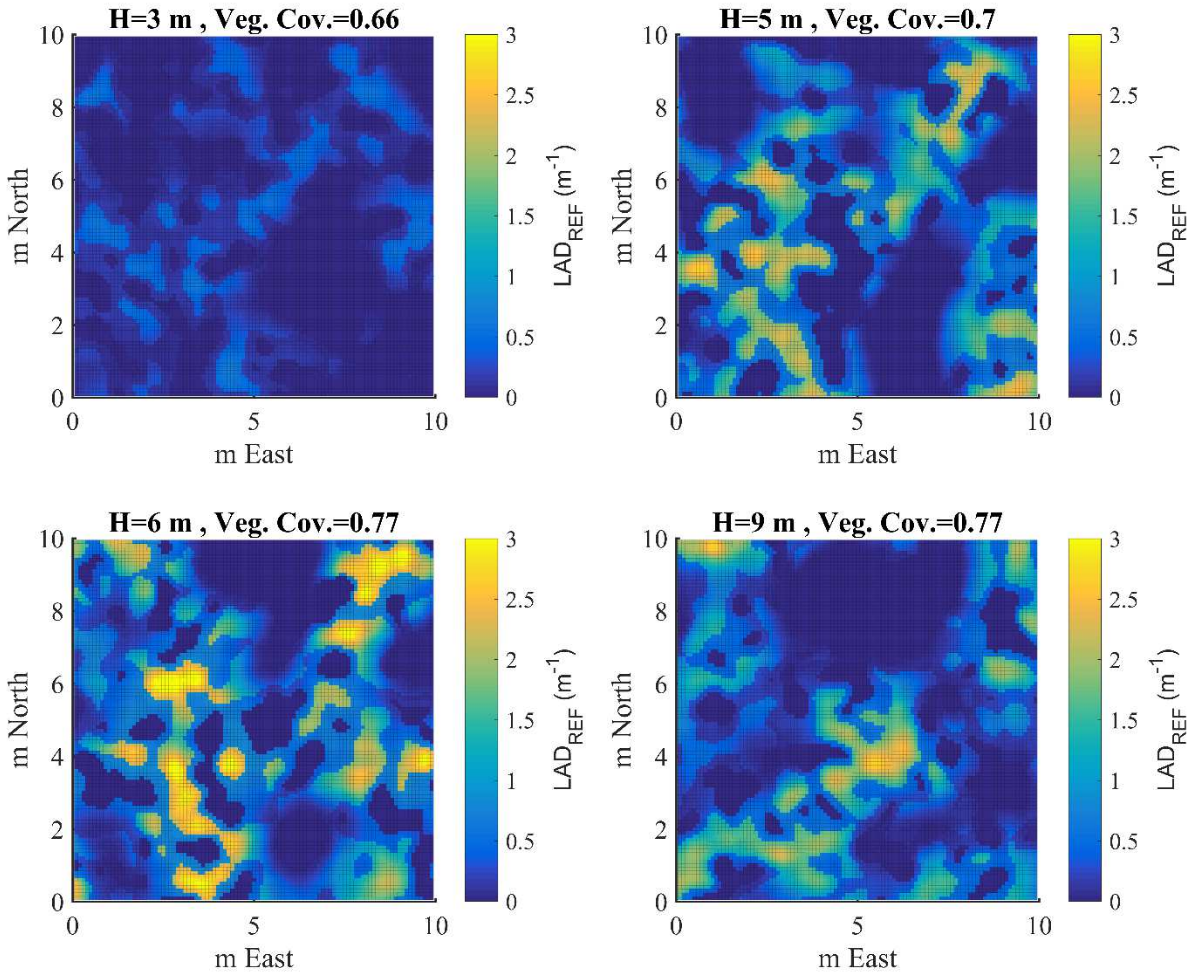

Figure 2. Reference horizontal distributions of LAD_{REF} at 4 different heights. Heights (H) of the mapped layer and associated vegetation cover fractions are indicated in titles. Colors are scaled on LAD_{REF} values from low to high densities (blue to yellow, respectively). A three dimensional view is available in Appendix C.

2.3. Simulation of a virtual point cloud corresponding to LAD_{REF} field

Simulation of virtual point clouds were based on turbid media assumption, which states that the probability of a beam to be intercepted increases exponentially with the optical depth (product of attenuation coefficient and distance travelled). The locations in which individual laser beams are intercepted are thus generated from the simulation of free paths (distance travelled before interception) from random numbers following probabilistic laws which account for vegetation density, as done for example in Pimont et al. (2018) within a single voxel. Here the approach is generalized to a heterogeneous scene, corresponding to an idealized forest plot with a spatially-correlated LAD field. The process is iterated in the different voxels travelled along the beam pass, for all beams according to the shooting pattern of the instrument representative of TLS field sampling of a forest plots.

2.3.1 Effective attenuation coefficient $\lambda_{eff,j}$ corresponding to a given scan j

The reference vegetation scene is the voxelized *LAD_{REF}* distribution described above. For simplicity, we assume that the size of vegetation elements (Beer law's approximation) and the volume of voxel occupied by wood elements are negligible. This allows simple framework adequate for testing sampling effect at stand-scale, but both factors can be rigorously accounted for, as shown in Pimont et al. (2019). As detailed above (Eq. 1), the reference attenuation coefficient $\lambda_{eff,j}$ related to LAD_{REF} for a given scan j depends on leaf projection, leaf fraction, vegetation heterogeneity and scanner properties. Yet, the probability of interception of laser beams depends exclusively on $\lambda_{eff,j}$, not directly on LAD_{REF}. To proceed to a realistic point cloud simulation and account for various distances between voxels and scan positions, the $\lambda_{eff,j}$ has to be computed at each voxel for each viewpoint j according to Eq. 1.

Let (x_j, y_j, z_j) be the coordinates of the scanner corresponding to scan j and (x, y, z) the coordinates of the center of a voxel in the vegetation scene. Following Eq.1 and according to the vegetation definition above, the effective attenuation coefficient for both leaf and wood for scan j is:

$$\lambda_{eff,j}(x,y,z) = LAD_{ref}(x,y,z)\frac{G_j(x,y,z)}{F(z)H_j(x,y,z)} \tag{4}$$

A beam emitted from the scanner that would go in the direction of this point has the following projection function G (since $\cos(2\theta) = \cos(\theta)^2 - \sin(\theta)^2$):

$$G_j(x,y,z) = \frac{1}{2} + 0.4\frac{z}{h}\frac{\left(z-z_j\right)^2 - \left(x-x_j\right)^2 - \left(y-y_j\right)^2}{\left(x-x_j\right)^2 + \left(y-y_j\right)^2 + \left(z-z_j\right)^2} \quad (5)$$

We assumed that the distance effect (caused by an increase in effective footprint of the scanner, as identified in Soma et al. 2018)) have the following effect on the attenuation coefficient:

$$H_j(x,y,z) = 1 - 0.05\sqrt{\left(x-x_j\right)^2 + \left(y-y_j\right)^2 + \left(z-z_j\right)^2} \quad (6)$$

which expresses that vegetation area is overestimated by a factor 2 at a distance of 10 m to the scanner (H_j=0.5). The reference LAD_{REF} field used to compute $\lambda_{eff,j}$ in presented in Figure 2. at 0.10 m discretization level (see section 4.5 for details).

2.3.2 Point cloud simulations

From the effective attenuation coefficient distribution (Eq. 15), we can simulate a virtual point cloud based on free path distribution simulations, as explained below. We assumed that function in (Eq. 15) can be discretized in a 3D computational grid ($\lambda_{eff,j}$ assumed to be constant within a computation cell, its value being equals to (Eq. 17) with (x,y,z) from cell center coordinate) with vegetation elements much smaller than grid size (turbid medium assumption).

Five scans were simulated. For each scan configuration, scans positions were placed with respect to optimal scene sampling coverage, similarly as field experiment would be, with the potential exception of absence of dense vegetation under 3m. All scans were placed at 1 m from the ground. 4 scans were placed close to each corner of the plot and one scan at the center:

$(x_1,y_1,z_1) = (7.5,7.5,1)$; $(x_2,y_2,z_2) = (7.5,2.5,1)$; $(x_3,y_3,z_3) = (2.5,2.5,1)$;
$(x_4,y_4,z_4) = (2.5,7.5,1)$; $(x_5,y_5,z_5) = (5,5,1)$.

We also parameterized their shooting pattern as follows. Their angular resolution was 0.05° over the horizontal (ranging from 0 to 180°) and the vertical (ranging from 0 to 360°), so that each scan contains 66 million beams, which is typical of the resolution used in the field (e.g. Pimont et al. 2015). For each beam, we simulated its eventual hit position as follows: First, optical path (i.e. initial potential to pass through vegetation) of each beam was randomly simulated according to Beer-Lambert law (assuming infinitely small elements):

$$l = -\log(p) \tag{7}$$

with p a random number between]0;1[(i.e. initial random chance to be intercepted by vegetation).

We then computed the trajectory of this beam within the computation grid, from its initial position at scanner location, by computing the “amount” of optical path required to cross the next voxel. This amount was calculated by multiplying the effective attenuation coefficient of this voxel by the length of the segment corresponding to the intersection of the beam and the voxel. When the residual optical path of the beam was shorter than this amount, a hit occurred within this voxel at a location corresponding to this residual optical path. On the contrary, when the remaining optical path was greater than this amount, it means that the beam travelled farther than the voxel. The process was recursively applied to the next voxel, the “new” residual optical path corresponding to the remaining of the previous one. The process ends in case of hit or when a beam reached the bounding box of the computational grid. In this later case, the beam was never intercepted in the computational grid, thus corresponding to a beam with no hit. This process is similar to the one used by (Pimont et al., 2009) to simulate photons trajectories to compute the radiative transfer from a flame through a voxelized heterogeneous vegetation scene with a MonteCarlo approach.

This process was repeated for each scan position. Hence, five virtual point clouds were simulated in accordance with $\lambda_{eff,j}$, which accounts for both vegetation and instrument properties.

2.4. *Computation of LAD estimates for simulated point clouds including unsampled voxels*

For each viewpoint j, we used a traversal algorithm developed under Matlab software (The MathWorks, Inc., Natick, MA, USA). For each scan, intersections between each beam (i.e. line between hit and scan position) and the voxel grid were computed in order to retrieve the following metrics in each voxel: Ni_j the number of hits in the voxel, $\sum z_j$ the sum of free paths, $\sum_{hit} z_j$ the sum of free paths corresponding to hits only.

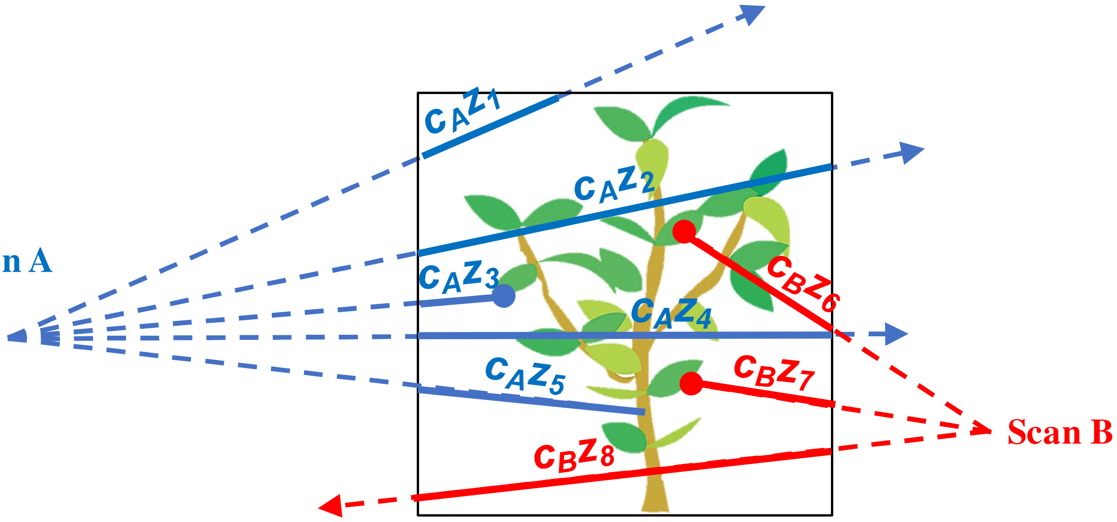

Figure 3. Scheme of the information provided by the traversal algorithm which is used to compute the unbiased estimator of *LAD* from multiview data from Scan A (in blue) and Scan B (in red): leaf hits (blue and red dots) and free paths (distances *z* travelled by the beams, blue and red lines) in the voxel. The dotted lines represent pulse trajectories. c_A and c_B represent the correcting factors for viewpoints A and B, which depend on distance to scanner and view angle (see Pimont et al., 2019 for details).

From these quantities, we can define in each voxel the following "multi scan" quantities, using known values of G, H and F:

- $\text{Ni} = \sum_j Ni_j$ the total number of hits
- $\sum \frac{G}{H} z = \sum_j \frac{G_j}{H_j} \sum z_j$ the total free path sum, with multiplicative correction factors.
- $\sum_{hits} \frac{G}{H} z = \sum_j \frac{G_j}{H_j}_j \sum_{hit} z_j$ the total "hit" free path sum, with multiplicative correction factors.

Following Pimont et al. (2019, Eq. 13), we used the following unbiased point estimator of LAD, provided that N was larger than 2:

$$\widetilde{LAD} = \frac{F}{\sum \frac{G}{H} z}\left(\mathrm{Ni} - \frac{\sum_{hits} \frac{G}{H} z}{\sum \frac{G}{H} z}\right) \tag{8}$$

In this formulation, $\frac{\sum_{hit} \frac{G}{H} z}{\sum \frac{G}{H} z}$ is a biais correction term ranging between 0 and 1, so that the estimator is simply $\frac{FNi}{\sum \frac{G}{H} z}$ when Ni is large, which corresponds to the Maximum Likelihood Estimator (Pimont et al. 2018). This formulation also accounts for leaf orientation, wood and instrument specifications (Pimont et al. 2019). This estimator generalizes the Modified Contact Frequency proposed by Béland et al. (2011) with the bias correction term to account for low sampling, leading to an unbiased point estimator provided that more than 2 beams are available (Pimont et al. 2018). The voxels with N smaller or equal to 1 were considered as unsampled, because no unbiased estimator has been suggested for N=1 (Pimont et al. 2019). Indeed, Eq. 8 leads to estimates of 0 when N=1, even when Ni=1, which is obviously negatively biased. As a result, voxels with N lower than 2 were considered as unsampled. For unsampled voxels, we used the “mean layer value” to estimate LAD, which was computed from the mean of $\widetilde{LAD}$ (computed for N larger or equal than 2). This method for dealing with unsampled voxels is the most widely used (Béland et al., 2014b; Schneider et al., 2019).

We also computed the radius of the 68% confidence interval for $\widetilde{LAD}$, which can be estimated by (Pimont et al. 2019):

$$\Delta\widetilde{LAD} = \frac{F\left(\mathrm{Ni} - \frac{\sum_{hits} \frac{G}{H} z}{\sum \frac{G}{H} z}\right) + \frac{1}{2}}{\sqrt{F\mathrm{Ni} + \frac{1}{2} \sum \frac{G}{H} z \left(1 + \frac{1}{N}\right)}} \tag{9}$$

with $N = \sum_j N_j$ the total number of beams entering a voxel.

2.5. Analysis of estimations

Table 1. Description of the different simulations. They differ both in the reference vegetation field used to generate the virtual point cloud (ray-tracing algorithm) and in the voxel size used for the estimation process.

Reference vegetation used to generate the virtual point cloud (scale in m)	*Voxel size used for estimation*	*Estimations*
LAD_{REF} (0.1 m)	0.1 m	$\widetilde{LAD}_{0.1}$
LAD_{REF} (0.1 m)	0.2 m	$\widetilde{LAD}_{0.2}$
LAD_{REF} (0.1 m)	0.5 m	$\widetilde{LAD}_{0.5}$
LAD_{REF} (0.1 m)	1.0 m	$\widetilde{LAD}_{1.0}$
$LAD_{REF\ s0.5}$ (0.5 m)	0.5 m	$\widetilde{LAD}_{s0.5}$

LAD_{REF} corresponds to the reference vegetation field defined at 0.1 m resolution. $LAD_{REF\ s0.5}$ corresponds to a manipulation of LAD_{REF}, which was smoothed at 0.5 m. As the scale of heterogeneity in these different reference fields differ, the subsequent virtual point clouds are also different.

2.5.1 Exploring bias arising from vegetation heterogeneity

It has been suggested that ignoring clumping effect within voxel could lead to strong LAD underestimation (Béland et al., 2014a; Soma et al., 2018). This bias depends on voxel size, large voxels being more prone to aggregate gaps and clumps within voxel volume. In the present study, we analysed the effect of voxel size by comparing estimates obtained with voxel sizes ranging from 0.10 m to 1 m to reference values (section 5.4). This analysis relied on mean estimated vertical profiles (i.e. estimates were averaged by height layers). For each voxel size, the correction factor required to match reference value was derived at all heights. One of the drawback of a basic sensitivity analysis to voxel size is that it does not disentangle the effects of vegetation heterogeneity (i.e. Jensen's inequality) and sampling limitations (i.e. more or less beams exploring voxels). In order to minimize the role of sampling limitations in the voxel size analysis, we only used estimations derived from the maximum sampling level, i.e. 5 scans design. To unravel the effect of subgrid vegetation heterogeneity, LAD estimations with 0.5 m voxels were performed both on original LAD_{REF} and on

$LAD_{REF\ s0.5}$. By definition, $LAD_{REF\ s0.5}$ field was manipulated (smoothing) so that it does not include any vegetation heterogeneity below 0.5 m. This result is presented in section 3.3. Then the magnitude of vegetation heterogeneity effect is characterized in section 3.4 by comparing LAD estimations retrieved with tested voxel sizes on vegetation resolved at 0.1 m scale (i.e. $\widetilde{\mathrm{LAD}}_{0.1}$ to $\widetilde{\mathrm{LAD}}_{1.0}$ compared to LAD_{REF}).

2.5.2 Consequences of sampling limitations

To provide insights regarding limitation associated with sampling in this context, we evaluated the sensitivity of estimates to the number of scans (different scan designs, from a single viewpoint to 5 scans) in sections 3.4. and 3.5. The single scan configuration used the scanner in central position, the two scans configuration used opposite diagonal design (top left to bottom right), the three scans configuration used full diagonal design and the four scans configuration used corners positions and five scan design used all positions.

Additionally, in order to perform a cross analysis between voxel size and number of scans, each scan configuration was used at both 0.10 m and 0.5 m voxel sizes. To disentangle the effect of sampling from the effect of vegetation heterogeneity (see 2.5.1), we used $LAD_{REF\ s0.5}$ field for LAD estimations with 0.5 m voxel (i.e. $\widetilde{\mathrm{LAD}}_{s0.5}$), similarly to section 2.5.1. Therefore, differences between estimates in section 3.5 cannot be attributed to a potential effect of vegetation heterogeneity effect, but only to sampling. Analyses of estimated vertical profiles were performed similarly to analysis of voxel size bias. For the computation of the vertical profile, we remind that the unsampled voxels were estimated by the "mean layer value". One should notice that in practice, LAD profiles computed from all voxels (including unsampled voxels estimated with the "mean layer method") provide identical profiles to those computed with means based on sampled voxels only.

All configurations were tested against references. Evaluations were performed through the comparison of mean layer $\widetilde{LAD}$ profile and mean absolute error (MAE). For a given set of voxels or layer i, MAE was computed according to:

$$MAE_i = \frac{\overline{|LAD_{REF,i} - \widetilde{LAD}_i|}}{\overline{LAD_{REF,i}}} \qquad (10)$$

Additionally, we analyzed the distribution of 68%-confidence interval radius (Eq. 9) to evaluate efficiency of local estimates for various scans and voxel sizes configurations.

3. Results

3.1. Overview of LAD patterns estimation

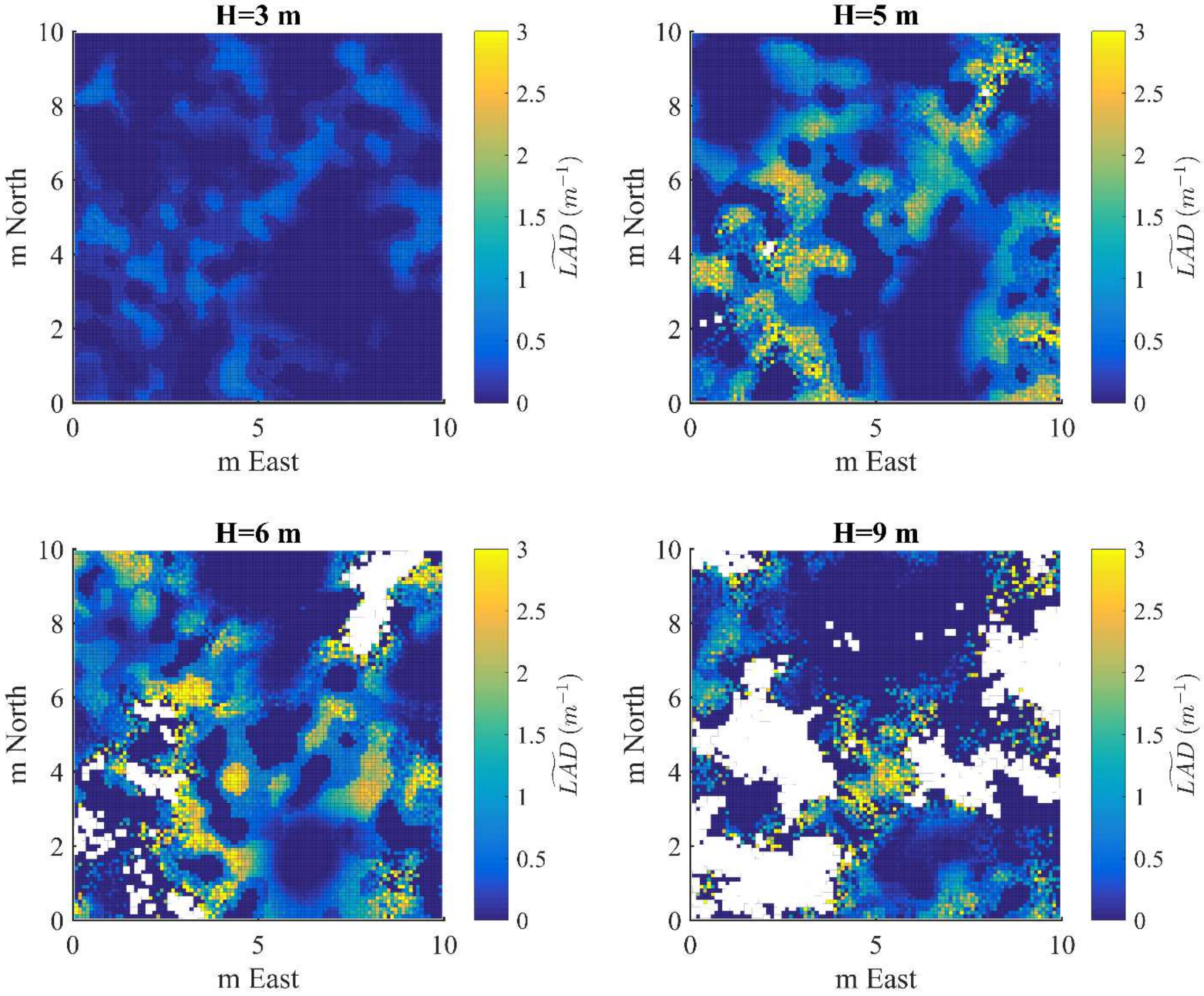

Figure 4. Estimated horizontal distribution of $\widetilde{\mathrm{LAD}}_{0.1}$ at four heights. Heights (H) of the mapped layer and associated vegetation covers are indicated in titles. Colors are scaled on $\widetilde{LAD}$ values from low to high densities (blue to yellow, respectively). These distributions can directly be compared to subplots

in Fig. 1 (LAD_{REF}). Here, the traversal algorithm was applied to the five scans at a 0.10 m voxel size. Blank pixels are unexplored voxels, which reveal occluded locations in the upper part of the canopy.

Figure 4 shows horizontal distributions of LAD estimations at four heights above ground level, providing insights on the 3D distribution of $\widetilde{\mathrm{LAD}}_{0.1}$ at plot scale. Comparison with the same plots shown for LAD_{REF} in Figure 2 allowed to identify main discrepancies with the reference field. At low height (H=3 m), estimates were very close to the reference for all voxels. From 5 m height and above, the general structure and variability in the LAD distribution was captured, but a few discrepancies can be identified. In particular, horizontal variations in $\widetilde{\mathrm{LAD}}_{0.1}$ were less smooth than the reference, with inaccuracy resulting from poor sampling. Typically, local differences were identified, mostly visible in dense clumps and a few voxels that were not sampled (in white). At 6 m height, some large blocks of unexplored voxels occurred, most of them being located in dense locations (LAD higher than 2 m^{-1}). In upper canopy (H=9 m), large errors occurred (higher than 100%) and unexplored voxels were very frequent (~30% of voxels). These unexplored locations were typically structured in large blocks (until 4-m width), covering both dense and light vegetation density.

The following sections provide quantitative analyses of estimations under various configurations.

3.2. *Influence of unsampled voxels (mean layer estimates)*

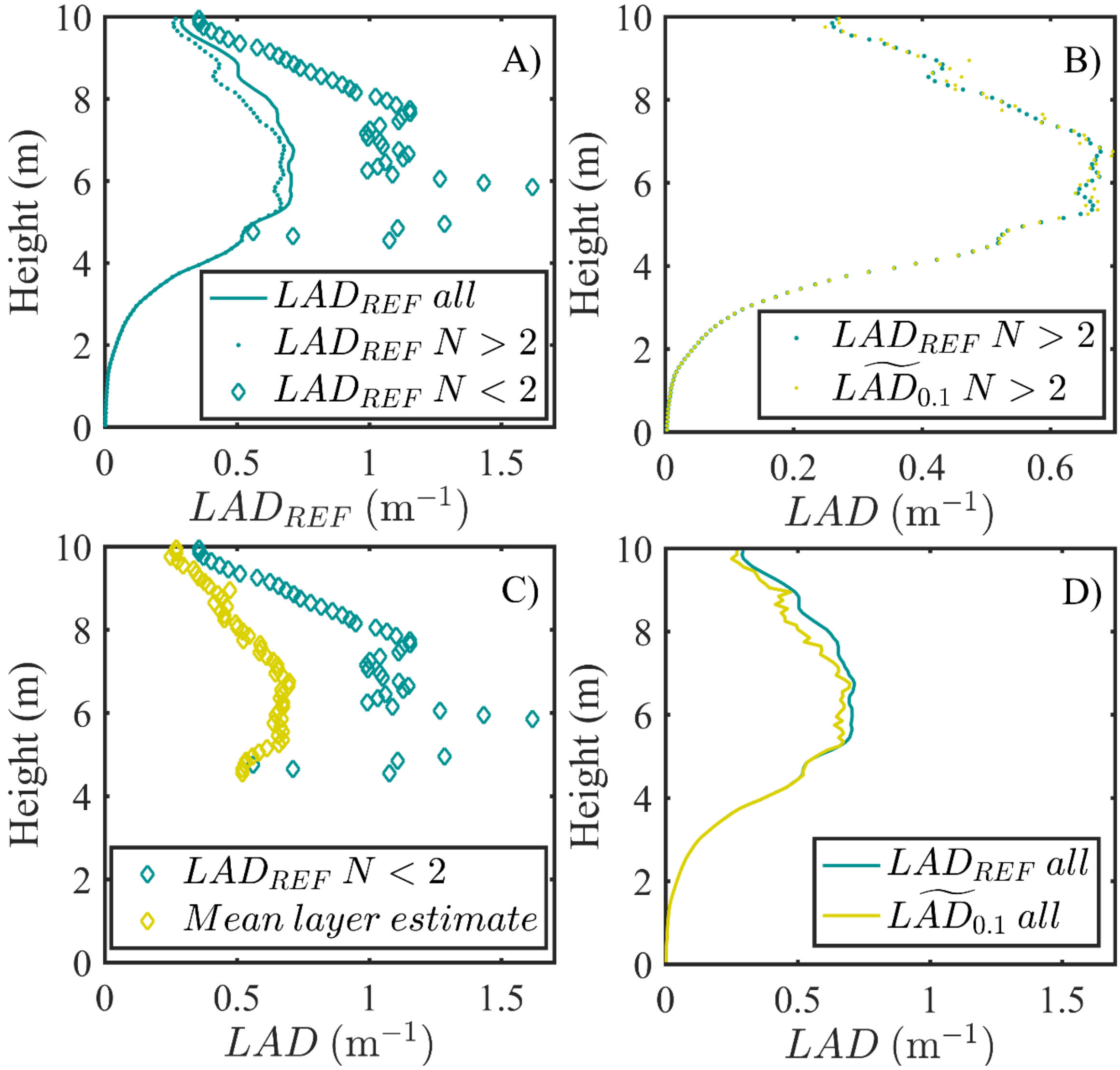

Figure 5. Comparison of LAD profiles at 0.1 m voxel size with 5 scans. A) Comparison of LAD_{REF} profiles for all voxels (blue curve), sampled voxels (N>2, blue dots) and unsampled voxels (N<2 (blue diamonds). B) Comparison of LAD_{REF} and $\widetilde{\mathrm{LAD}}_{0.1}$ from sampled voxels (N>2, blue and yellow dots, respectively). C) Comparison of LAD_{REF} and $\widetilde{\mathrm{LAD}}_{0.1}$ from unsampled (N<2, blue and yellow dots, respectively). D) Comparison of LAD_{REF} and $\widetilde{\mathrm{LAD}}_{0.1}$ profiles with all voxels (blue and red yellow, respectively).

In this section, we consider LAD estimations of LAD_{REF} at 0.1 m voxel size. Therefore, we must not expect any effect of subgrid vegetation heterogeneity on estimations, as this is exactly the resolution of the reference field. Figure 5 compares profiles obtained for references and estimated voxels, which were respectively explored by less or more than 5 beams. The analysis of reference profiles (**Fig5A**) allowed to pinpoint sampling quality differences depending on reference LAD values. As expected, the unsampled voxels at a given height exhibited systematically the highest reference LAD values, well above the mean LAD_{REF} (**Fig5A**), and were systematically underestimated, because the "mean layer" value (that was attributed to unsampled voxels) was strictly lower than actual references in unsampled voxels (**Fig5C**). For explored voxels, the agreement between the reference and the estimation was very good (**Fig5B**), which confirms the unbiasness of point estimates used in the present study (initially proposed by Pimont et al. 2018). This demonstrates that the overall underestimation (**Fig5D**) was caused by unsampled voxels (even if the "mean layer" value was assessed to these voxels). This confirms the hypothesis presented in introduction, where we suggested that the heterogeneity of sampling was likely to induce biases in mean estimates. Moreover, these differences in LAD_{REF} between sampled and unsampled voxels decreased in the upper part of the canopy (**Fig5A**). Hence voxels had similar averages near canopy top. This suggests that sampling restriction was a random process where occlusion was very severe (in the upper part), contrary to where occlusion began (mid canopy), where occlusion concerned more frequently the denser voxels.

3.3. Influence of subgrid vegetation heterogeneity

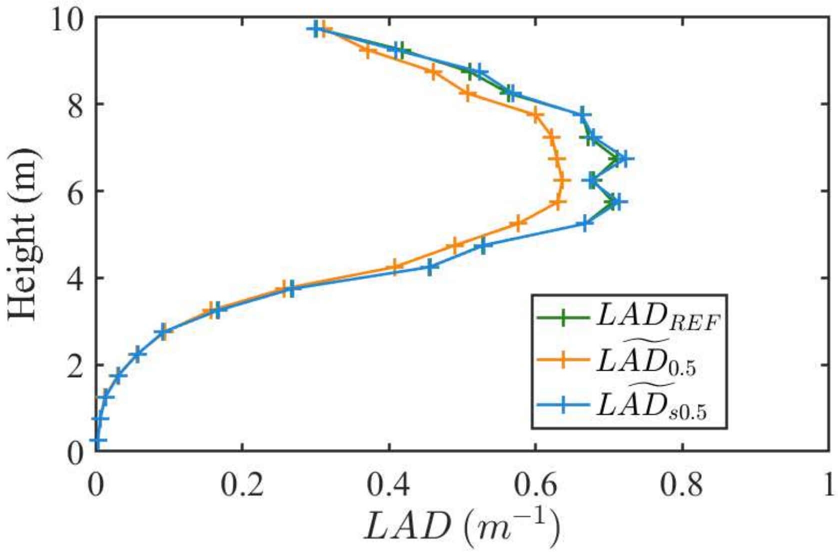

Figure 6. Comparison of five scans design profiles of $\widetilde{\mathrm{LAD}}_{0.5}$ and $\widetilde{\mathrm{LAD}}_{\mathrm{s}0.5}$ (generated from the smoothed reference $LAD_{REF\ s0.5}$) with the reference LAD_{REF}. Profiles were averaged in 0.5-m layer to ease comparisons, so that a single reference could be used for both estimates (labelled LAD_{REF} for simplicity), as $LAD_{REF\ s0.5}$ and LAD_{REF} were identical at the 0.5 m resolution by definition.

At coarser voxel sizes, convexity effects associated with subgrid vegetation heterogeneity are expected to affect LAD estimations, also leading to underestimations when, for example, comparing $\widetilde{\mathrm{LAD}}_{0.5}$ to references (Figure 6). However, a part of this negative bias could have been caused by the presence of unsampled voxels. In order to formerly attribute this negative bias to subgrid vegetation heterogeneity, we used the estimates ($\widetilde{\mathrm{LAD}}_{\mathrm{s}0.5}$) derived from smoothed reference fields $\mathrm{LAD}_{\mathrm{REF\ s}0.5}$ (Figure 6), corresponding to a scenario in which no subgrid vegetation heterogeneity can occur. In this case, estimates ($\widetilde{\mathrm{LAD}}_{\mathrm{s}0.5}$) were very close to reference profile, demonstrating that the role of the sampling bias was negligible in this scenario. The negative bias observed with $\widetilde{\mathrm{LAD}}_{0.5}$ was hence attributed to subgrid vegetation heterogeneity.

3.4. *Overall sensitivity of estimation to voxel sizes*

Because subgrid vegetation heterogeneity and sampling depends on voxel size, the amplitude of negative biases is expected to vary with voxel size, which is investigated in next section.

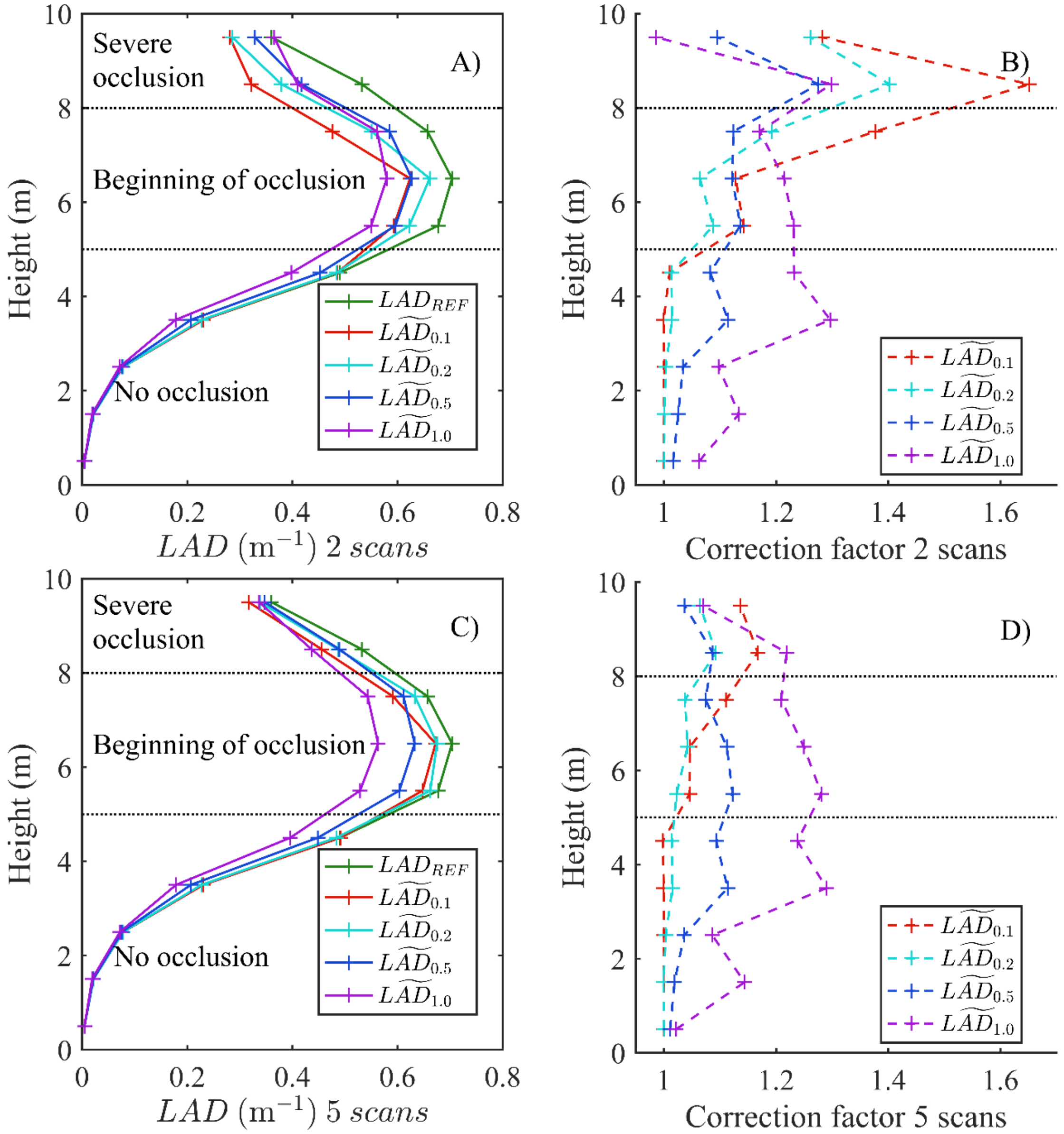

Figure 7. A) Vertical profiles retrieved with $\widetilde{LAD}$ estimates with various voxel sizes for the two scans design. B) Vertical profiles of the multiplicative correction coefficient required to retrieve reference value ($\frac{LAD_{REF}}{\widetilde{LAD}}$) using the two scan design. C) and D) Same as A and B, but for the five scans design. In these plots, LAD were averaged in 1-m layer when voxel size was smaller than 1 m to ease comparison between estimates across voxel sizes. Dotted lines roughly pinpoint height boundaries between layers with no occlusion, layers where occlusion starts to occur (typically within vegetation clumps) and layers with widespread occlusion patterns (both within and outside vegetation clumps).

In Figure **7A**, we show the overall sensitivity of estimates of $\widetilde{LAD}$ profiles to voxel size, including both sampling and subgrid vegetation heterogeneity biases, for two scans and five scans designs. All voxel sizes adequately captured the shape of the reference profile. However, various amplitudes of underestimations were observed depending on voxel sizes, scan design and height in the canopy. The significance of these effects was confirmed by a statistical analysis (Appendix D). In well explored layers, i.e. below 5 m, coarser voxel sizes led to strong underestimations, requiring highest correction factors for both scan designs. However, as occlusion occurred and increased in highest layers, the two smallest voxel sizes yielded strongest and variable underestimations, of greater magnitude than with the 0.5 m and 1 m voxel sizes (7B). On the contrary, even in mid and top layers, the biases observed with 0.5 m and 1 m voxel sizes were similar to those below 5 m, resulting in a relatively homogenous bias in the whole canopy.

According to the results of previous sections 3.2 and 3.3, underestimations resulted from two different mechanisms, namely, sampling bias for small voxels (e.g. 0.1 m, **Fig 5**) and convexity bias associated with subgrid vegetation heterogeneity for coarse voxels (e.g. 0.5 m, **Fig 7**). Our analysis and vegetation manipulation allowed to disentangle and quantify these biases. We found that their magnitude and their spatial distribution was variable, but that bias arising from sampling limitations was very unstable and of stronger magnitude.

3.5. Sensitivity of estimates to variations in sampling design (without subgrid heterogeneity effect)

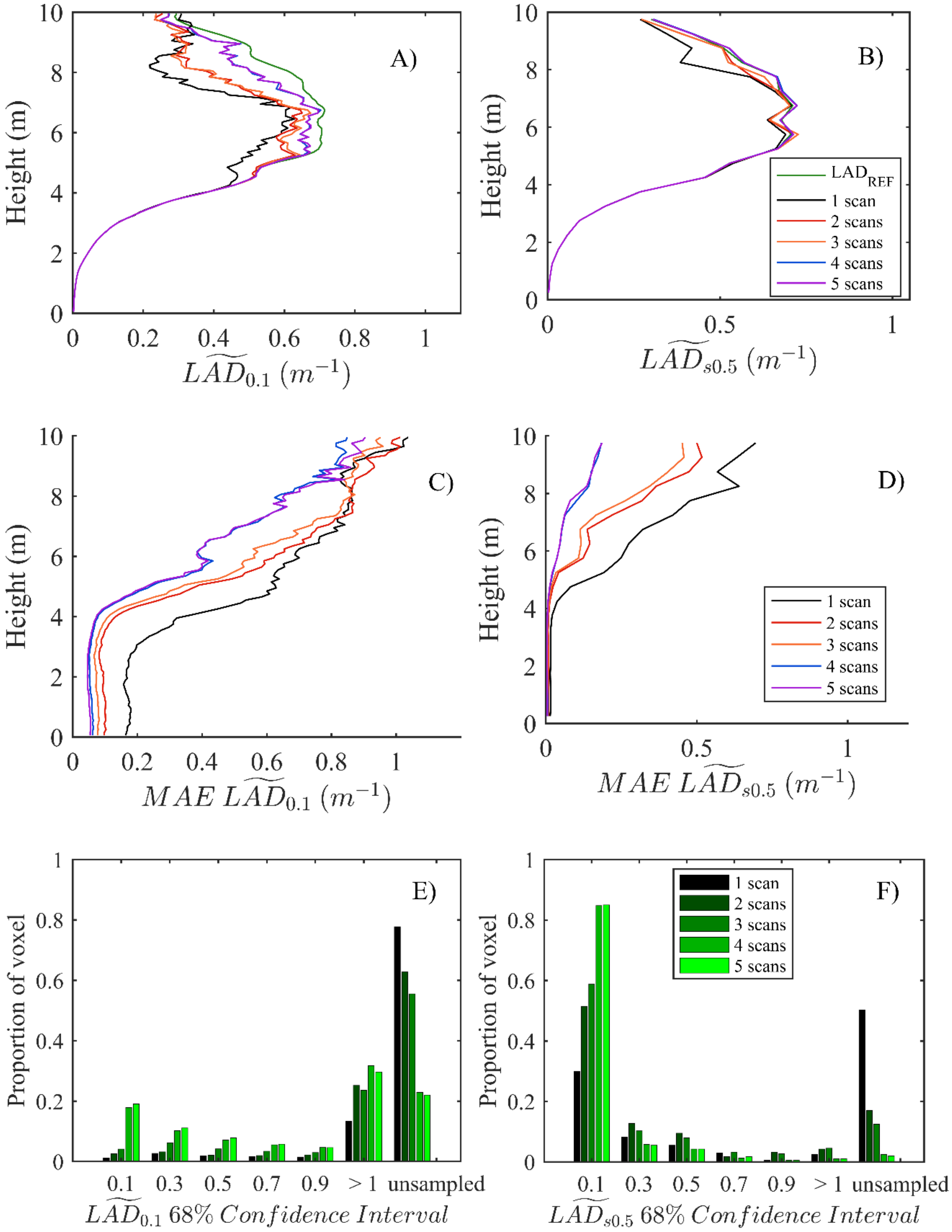

Figure 8. A. Vertical profiles of $\widetilde{\text{LAD}}_{0.1}$ for 1 to 5 scan design. B. Vertical profiles of $\widetilde{\text{LAD}}_{\text{s0.5}}$ for 1 to 5 scan designs. Profiles of Mean Absolute Error (MAE, in fraction) are presented accordingly for each voxel size for $\widetilde{\text{LAD}}_{0.1}$ and $\widetilde{\text{LAD}}_{\text{s0.5}}$ in subplots C) and D), respectively. MAE were normalized by the mean reference values within each horizontal layer. Distributions of 68% confidence intervals

with 1 to 5 scan designs (colored bars from black to green, respectively) for $\widetilde{\mathrm{LAD}}_{0.1}$ and $\widetilde{\mathrm{LAD}}_{s0.5}$ in subplots C) and D), respectively. Bins have a 0.2 m^{-1} extent centered on x-axis labels.

Figure 8. presents $\widetilde{LAD}$ profiles and corresponding Mean Absolute Error (MAE), for various number of scans (1 to 5 scans design) and two voxel sizes (0.1 m and 0.5 m). Normalized MAE inform on the accuracy of the estimation at voxel scale. For the coarsest resolution, we use the smoothed reference field to eliminate the subgrid vegetation heterogeneity effect.

The shape of the reference profile was roughly captured for all scan designs and voxel sizes (**Fig. 8AB**). Below 8 m, estimations were closer to reference (**Fig. 8AB**) and errors decreased as the voxel size and/or the number of scans increased (**Fig. 8CD**). The negative bias was less pronounced in the upper part of the canopy (above 8 m), as already noticed with large voxels (**Fig 7**), with more randomly distributed occlusion voxels (with regards to voxel density). For example, the bias was the same for 5 and 1 scans for the 0.1m voxel size in the upper part of the canopy (**Fig 8A**). Both 4 and 5 scans design yielded relatively close estimates to the reference, but their MAE were very poor in upper canopy layers (~100% error), remaining similar to the single scan design MAE (**Fig 8C**). At 0.5 m voxel size (**Fig 8B**), with the 4 and 5 scan design, the estimated profile (blue and violet lines) closely matched the reference. In this context, coarser voxels exhibit an increased sampling rate with respect to fine voxels (as for multiplying scan positions), leading to significantly better estimated profiles and smaller MAE values (thanks to the suppression of the subgrid vegetation heterogeneity effect). However, the single scan design, and in a lesser extent 2 and 3 scans designs, remained affected by systemic negative bias and large occlusion (drop down of estimations) above 8 m, even with 0.5 m voxels (**Fig 8B**). Conversely to 1-2-3 viewpoints, MAE were much lower than with 0.1 m voxel size and were limited to 0.7 at top height, which showed that the estimated local voxel value was more reliable. Remarkably, the 4-5 scans design had MAE limited to 0.2 at top height, which is consistent with a 20% error on a given voxel in average.

Figure **8EF** shows the impact of number of scan and voxel size on the distributions of 68% confidence intervals (CI) in sampled voxels, and on the occurrence of unsampled voxels. Increasing the voxel size and number of scans decreased occurrences of unexplored voxels, as suggested above.

In particular, 80% of voxels were unexplored for a single scan at 0.10 m voxel size (i.e. most critical case), implying that estimations relied on only 20% of the vegetation scene. More generally, more than 50% of the voxels are unexplored when three scans or less are used, which highlights that such a 0.1 m voxel size is not really practical given TLS resolution and number of scans.

For explored voxels, increase in number of scans and voxel sizes tends to decrease CI width, leading to higher frequencies of small errors. In particular, whatever the scan design, increasing the voxel size shifted the occurrence of largest CI (>1) and unexplored voxels (i.e. infinite error) towards the lowest CI values. Typically, the single scan design was almost unable to produce estimations with CI lower than 1 m^{-1} at 0.10 m voxel size, whereas 30% of estimations reached the smallest confidence level with 0.5 m voxel size. Similarly, with the 4-5 scan designs, 20% of the estimates had the smallest confidence level at 0.10 m voxel size, while 85% of voxels are estimated with CI lower than 0.2 m^{-1} at 0.5 m voxel size. As a result, at least 50% of the voxels were unexplored with the 0.1 m voxel size, even for 5 scan designs. These points highlight the fact that the sampling used in the present numerical experiment, which was representative of field conditions (a few scans per forestry plot, with 0.036° resolution) was too limited to provide reliable results at the 0.1 m voxel size, contrary to coarser voxels, which on the other hand, raise the problem of subgrid vegetation heterogeneity (**Fig 6**, **Fig 7**).

4. Discussion

The simulation framework used in this study allowed to evaluate the process of estimations of LAD with TLS thanks to exact references. In particular, we analysed the sensitivity to vegetation and sampling heterogeneities. We disentangled combined effects associated with variations in voxel sizes and scan designs with respect to true numerical references, and biases were formerly attributed to two main mechanisms, thanks to our numerical design and the used of unbiased point estimators. Our study confirmed the effect associated with subgrid vegetation heterogeneity, which leads to underestimation when voxels are too coarse to explicitly account for it. This effect is discussed in section 4.1. Our study also demonstrates that an overall negative bias can arise when relying on mean layer estimates for correcting for the presence of unsampled voxels. The bias was not homogeneously distributed within the vegetation scene and typically occurs when occlusion begins to be significant (at mid-canopy height in the present example), as it more frequently affects clumps of dense voxels, but can diminish in highest vegetation layer, despite strong occlusion. This effect is discussed in section 4.2. Beyond overall biases in vertical profiles, we also studied the sensitivity of voxel-scale predictions to voxel size and scan design, as the objective of voxelized TLS method is to measure the tri-dimensional distribution of the LAD. The distribution of confidence intervals showed that the voxel sizes required for a reasonable accuracy (here typically 0.5m), could be larger than the voxel size required to mitigate subgrid vegetation heterogeneity. The discussion ends with recommendations and future work.

4.1. Subgrid vegetation heterogeneity should be accounted for to provide reliable estimations

In the present study, underestimations occurred when voxel size increased (i.e. 0.5 m, **Fig. 6**), and the negative bias of the estimated LAD profile (i.e. for a horizontal layer of voxels) could reach 30% for 1 m voxel size (**Fig. 7**). We found that such underestimation did not occur when point clouds were generated with vegetation that was smoothed at voxel size ($\widehat{\mathrm{LAD}}_{\mathrm{S}0.5}$, **Fig. 6**), which demonstrated that this effect was caused by subgrid vegetation heterogeneity. This confirms prior observations on natural branches of three different species scanned with two different instruments (Soma et al., 2018), but also on trees (Béland et al., 2014a), which already attributed underestimations to vegetation heterogeneity. One can notice that the effect of voxel size observed in Soma et al. (2018) was more important, requiring a 1.7 correction factor with 0.7 m voxels compared to 1.3 for 0.5 m voxels in the present simulations. Such differences could arise from more heterogeneous vegetation structure in natural vegetation than in our example reference field, in which heterogeneity was resolved at 0.1 m scale. However, these findings demonstrate the efficiency of numerical experiments for testing hypothesis and evidence the associated mechanism (here heterogeneity effect on LAD estimation), since it was possible to numerically manipulate vegetation (here smoothing), for a formal attribution of bias source.

Similarly to approaches developed for passive optical measurements (e.g. hemispherical photography), identifying canopy gaps and angular segmentation the scene is efficient to partially correct for clumping (Yan et al., 2019). Yet, the subgrid vegetation heterogeneity in each segment of 2D images remains along the optical depth, i.e. in the third dimension. Our results illustrate the potential of an appropriate segmentation level to limit the clumping effect, making TLS voxel-based approaches more efficient compared to 2D gap fraction methods for the separation of gaps and crowns and particularly fitted for application of LAI retrieval approaches, including path length distribution models whether at crown (Hu et al., 2018) or voxel scales (Pimont et al., 2019; Soma et al., 2018).

4.2. Sampling limitations generate heterogeneous and variable underestimations

When occlusion was limited (typically 5 scans and 0.5 m voxel size), the clumping effect was the main source of underestimation in LAD. However, when sampling limitation became significant, typically above 5 m and with 0.1 m voxels ($\widetilde{\mathrm{LAD}}_{0.1}$, **Fig 7AB** – red curve), underestimations of heterogeneous magnitudes occurred without any subgrid heterogeneity, demonstrating the presence of a second mechanism of underestimation. This negative bias arose from the spatial correlations between sampling limitations and LAD densities, as clumps of dense volumes were more frequently occluded. Indeed, scan positions located in the open ease the sampling of empty or light voxels and might amplify the oversampling of light voxels described above, while dense voxel are rarely explored and less accounted for in mean layer LAD calculation. This spatial structure of occlusion can result in up to 25% underestimations (**Fig. 8A**) of the average LAD profile despite 5 scans are performed. In these non-sampled volumes, we assigned the mean layer estimated values, which results from sampled voxels in dense layers, i.e. mostly empty and low density voxels, generally equal to 0.4 m^{-1} in average, i.e. much less than dense voxel LAD values. As less and less beams coming from below canopy remained available in the canopy middle, clumps of dense occluded voxels are more frequent, and such underestimation mean bias was worse until 8 m height. Above 9 m, this bias was dampened (**Fig. 8AB**), because the correlation between dense voxels and occluded area is much less pronounced. In other words, large spots of unexplored voxels in top-canopy affected almost randomly both empty and dense above volumes (**Fig. 4**). As a result, such strong exposure to occlusion led to underestimations of significant but very heterogeneous magnitudes along vertical profiles (Fig 7B). It suggests that such underestimations depend on both the canopy structure and the degree of occlusion, which are both hardly predictable. On the contrary, coarser voxel sizes were much less affected by occlusion, and were rather affected by a significant but spatially homogenous negative bias attributed to clumping effect. In these conditions, it seems a better strategy to avoid erratic negative biases resulting from the strong occlusion inherent to small voxel size by using coarser voxel sizes corrected for a more constant and measurable bias and less prone to large occlusion spots.

However, independently of the voxel size, such a negative bias is expected to systematically occur in layers where occlusion starts, as soon as the dense voxels are clumped. Thus the “mean layer” method for dealing with unsampled voxels is not satisfying. Additionally, it raises sharp errors locally.

Strong underestimations at layer and plot scales are in accordance with previous observations from ground perspectives (Schneider et al., 2019). Increasing the number of scans and the voxel size limited occurrence of unexplored voxels, so that estimations were generally improved. However, highest number of scans with smallest voxel size or single scan with 0.5 m voxel size were still affected. Hence, the appropriate combination of scan design and voxel size directly depends of the vegetation density and of the level of detail required to match user’s aim. Typically, retrieving LAD profiles shapes and values with 20% error can be achieved either by 5 scans with 0.1 m voxels or by a single scan with 0.5 m voxels in sparse vegetation structures **(Fig 8AB)**. However, in dense vegetation and/or when estimates at voxel scale are valuable (i.e. for 3D radiative transfer modelling), it seems mandatory to rely on both multiple viewpoints and coarse voxels to retrieve unbiased estimates and reliable voxel LAD value (**Fig. 8CD**). Similarly to (Schneider et al., 2019), until 80% of voxels can be occluded in critical cases **(Fig. 8EF)**.

By calculating confidence intervals at voxel scale, our study gives insights on the drop in local accuracy within voxel resulting from poor sampling conditions. This differs from the usual approach for quantifying occlusion consisting in counting voxel with at least one beam passing through, thus ignoring errors generated in poorly sampled voxels. Confidence intervals indicated that estimations in poorly sampled voxel can be affected by 1 m^{-1} errors, which is considerable regarding the range of reference LAD values. These confidence intervals can be considered as a statistical alternative to the use of mean nearest neighbour point (Wilkes et al., 2017) in order to assess the sampling densities of given areas, in particular when used approaches are sensitive to non-uniform distribution of points (i.e. for geometrical modelling of trees). Small voxels were frequently affected by large errors, until 35% of the scene. With the 4-5 scans design with 0.1 m voxels, CI > 1 m^{-1} are even more frequent than with a single scan (**Fig 8E**). This higher frequency of large CI was due to the poor exploration of voxels which would have remained unexplored with a single scan, producing unreliable estimates. Locally, such errors were worse than replacing estimates by the mean layer value, suggesting that the reduction of occluded voxel percentage should not be the single criteria for sampling accuracy, and raised the question of the appropriate criterion for occlusion. Determining whether to replace voxel by a fixed value or to keep the estimation given by few beams is particularly difficult in clumped situations given the strong correlation observed between occlusion areas and high LAD values areas. This advocates for the development of correction techniques that are not based on numerical thresholds (Soma et al. 2020).

4.3. Recommendations and research needs

All identified estimation biases were negative. The vegetation heterogeneity effect could yield up to 20% underestimations (**Fig. 6**, **Fig. 7BD**), while unsampled voxels led to profiles that could be locally less than half of reference (**Fig. 8A**), and even worst locally. In the field, these negative biases are entangled and add up, which can potentially induce a global stronger bias than observed in these simulations. Hence, these biases should not be overlooked and we strongly recommend to limit their magnitude and correct them when possible. This study confirms observations of Béland et al., 2014a at the scale of individual trees, i.e. increasing voxel size is an efficient way to level up sampling at voxel scale. Such coarser discretization level should be considered with caution, as it leads to the aggregation of gaps and clumps, as well as the aggregation of occluded and explored areas in same voxels. However, negative bias resulting from occurrence of occlusion are unstable and of higher magnitude and should be avoided in first place, suggesting coarse voxel sizes remain an advantageous option. To determine the appropriate voxel size, the ability to correct for subgrid vegetation heterogeneity (Soma et al., 2018) and to assess accuracy with confidence intervals are key steps.

In light of our results, we recommend to use unbiased estimators and to rely on multiple viewpoints. Tested vegetation scene had a 10 m extent in each dimension, with no or few vegetation below 3 m height. The density of scans was relatively high (2.5 m between scans) compared to other studies (Schneider et al., 2019; Wilkes et al., 2017). However, the simulated vegetation features, which were representative of Mediterranean canopies (Simioni et al., 2016), displayed much denser clumps of LAD values (0.6 m^{-1} in average) compared to retrieved LAD in other vegetation types (~ 0.3 m^{-1}). In such dense context, occlusion occurred from 5 m height, while accurate sampling has been observed until 35-m height with multi-echoes instrument and in other field conditions (Schneider et al., 2019). This proves that *a priori* recommendations concerning visibility analysis can hardly be applied to a range of vegetation structures and different forest types. Providing exhaustive guidelines based on easily measurable stand parameters, i.e. number of large stems (Abegg et al., 2017), presence of understorey or mean crown width could help to plan appropriate scan design across sites. Additionally, the terrestrial LiDAR simulated in this study was a single echo scanner, typically representative of the FARO Focus 3D, which is used in operational context for French forest monitoring. Other scanners, such as RIEGL VZ400, a multi-echoes LiDAR, have better exploration skills and are less sensitive to occlusion. Then, as suggested in (Wilkes et al., 2017), recommendations should also be adapted to the type and resolution of instruments. Yet, beam density also decreases at a given distance of these multi-echoes instruments, so that such scanners are theoretically exposed to the same bias arising from occlusion, as confirmed by observations in tropical canopies (Schneider et al., 2019). The bias arising from subgrid vegetation heterogeneity is independent of sampling accuracy and, as a result, concerns all instruments. The presence of vegetation in the lower part of the canopy (understorey) might generate more occlusion, requiring to increase the number of scans. Hence, a particular attention should be paid to set instrument in order to obtain viewpoints that enable to efficient plot sampling, for example in open locations (Wilkes et al., 2017). Since the number of scans can generally not be increased in field conditions, a trade off on voxel size must be found. Therefore, we recommend to use medium voxel size, typically close to 0.5 m, with an empirical correction to account for vegetation heterogeneity in the subgrid volume. Scanning from the above perspective (i.e. UAV LiDAR) can provide significant reduction of occluded areas close to tops of canopies, but suffered from a limited penetration of beams in the mid-crown (Morsdorf et al., 2018; Schneider et al., 2019), so that similar negative biases associated with unsampled voxels and subgrid vegetation heterogeneity as identified in the present study should exist.

In the present study, we used the mean layer assumption (replacing unsampled voxels by the mean of LAD estimates obtained at corresponding layer) to extrapolate missing data. Such method is theoretically similar to ignoring these missing values in spatial averages, and suffer from strong local inaccuracy in dense or empty areas differing from mean LAD value. Additionally, poorly sampled voxels had frequent unreliable estimates, which might be locally more erroneous than replacing by the biased mean layer value. First, it shows the benefit of quantifying uncertainties of estimations in locations of interests (i.e. dense voxels), which should be included in further analysis when estimating LAD. Second, it raises the question of the definition of an occluded voxel.

In our numerical experiment, the leaf orientation factor, the leaf fraction, and the distance effect were known and corrected so that our estimators of the LAD were unbiased in each voxel to limit confounding errors in the numerical experiment. However, such parameters are challenging to retrieve in field conditions and their estimations are expected to induce errors (Yan et al., 2019), which might affect the outcome of the present study. The leaf orientation factor can be for example retrieved by leaves triangulations if LiDAR resolution is fine enough (Bailey and Mahaffee, 2017). Several classification methods have been proposed to classify leaves *versus* wood hits (Wang et al., 2020). Then, the leaf fraction factor can be retrieved as the ratio between leaves and total number of points in a given voxel. Eventually, the effect of the distance to scanner can be either estimated from laboratory experiments (Soma et al. 2018) or physical modelling of beam divergence (Béland et al., 2011). The occlusion bias highlighted in the present work should also be explored in other vegetation scenes with absolute references, e.g. with point clouds arising from the sampling of 3D tree models. We showed that underestimations constantly affected dense voxels where occlusion begin, but that voxels can be affected independently of their vegetation density in background and/or top layers, including empty areas. The consequences of this sampling bias in those partially explored layers directly depend on the representativeness of remaining sampled voxels, which can either results in top profile overestimations, underestimations or even in a limited bias. Then, we recommend to analyse the magnitude of this bias for a variety of vegetation structures in light of optical depth and correlation length in vegetation (Appendix B). This variability in spatial bias distribution, vegetation structure and the difficulty to define an occluded volume demonstrate the need for spatially adaptive methods to deal both with poorly sampled and fully occluded voxels. Given the clumped structure of vegetation, using the information of surrounding voxels is a promising approach. Such method relying on kriging has been developed and tested both on a virtual scene (e.g. in Appendix B), and then applied to field data (Soma et al., 2020). Corrections yielded encouraging results with a buffering of errors due to sampling limitations and a more adaptive guess of unexplored voxels values, holding the potential to retrieve better voxel and plot LAD estimations.

5. Conclusion

The present work disentangles some of biases related to LAD estimations with TLS through a numerical study. This simulation framework was mandatory to fully understand and quantify the magnitude of these major biases, because they mainly occur in dense and clumped canopy context, for which field references are often not available. Moreover, such a design allows vegetation manipulation, such as smoothing to ease analysis. First, simulations allowed to characterize a negative bias for LAD estimation due to subgrid vegetation heterogeneity in voxels, arising from dense and light density areas being encompassed within same volumes. Second, we assessed sampling accuracy with confidence intervals and identified a spatial correlation between occlusion and dense LAD in layers where occlusion of the laser beams starts to occur. This spatial correlation leads to underestimation of LAD profile, even when the mean layer value was attributed to unsampled voxels. Several methods to limit occurrence of unsampled voxels and increase sampling rate were efficient to damper underestimations. We confirm that combining the information from several scan positions was critical to improve the reliability of estimates. Moreover, the negative bias arising from unsampled voxels was prone to large and unstable variations of magnitude depending on the canopy structure. Then, we recommend to solve in first place the occurrence of unsampled areas, typically by using estimations from coarse voxels complemented by an adequate treatment of subgrid vegetation heterogeneity effect. In the present study, we found that at least 0.5 m voxel size was appropriate, with a mandatory correction for vegetation heterogeneity. The development of methods to extrapolate or correct LAD values in occluded volumes (e.g. kriging) remains a challenging but critical need. The simulation framework developed in our study cannot serve as sole reference for quantifying the magnitude of similar biases occurring with the diversity of natural vegetation and acquisition parameters, as many uncertainties that are inherent to the field conditions are neglected in numerical experiments. Yet, this study paves the way for additional research and field measures needed to characterize in operational context the biases identified in these simulations.

Author Contributions

M.S. conceived and designed the experiments; M.S. performed the experiments, as well as the analyses, with useful guidelines of F.P. and J-L.D. . M.S. wrote the paper, with critical contributions of the other co-authors.

Funding

This research was funded by Institut National de la Recherche Agronomique (INRA) and by Conseil Régional Provence-Alpes-Côte d’Azur (LiDARForFuel, grant n◦ APR-EX 2014_04163 and PhD grant n◦ 2015_07468).

6. References

Abegg, M., Kükenbrink, D., Zell, J., Schaepman, M.E., Morsdorf, F., 2017. Terrestrial laser scanning for forest inventories-tree diameter distribution and scanner location impact on occlusion. Forests 8. https://doi.org/10.3390/f8060184

Bailey, B.N., Mahaffee, W.F., 2017. Rapid measurement of the three-dimensional distribution of leaf orientation and the leaf angle probability density function using terrestrial LiDAR scanning. Remote Sens. Environ. 194, 63–76. https://doi.org/10.1016/j.rse.2017.03.011

Béland, M., Baldocchi, D.D., Widlowski, J.L., Fournier, R.A., Verstraete, M.M., 2014a. On seeing the wood from the leaves and the role of voxel size in determining leaf area distribution of forests with terrestrial LiDAR. Agric. For. Meteorol. 184, 82–97. https://doi.org/10.1016/j.agrformet.2013.09.005

Béland, M., Widlowski, J.L., Fournier, R.A., 2014b. A model for deriving voxel-level tree leaf area density estimates from ground-based LiDAR. Environ. Model. Softw. 51, 184–189. https://doi.org/10.1016/j.envsoft.2013.09.034

Béland, M., Widlowski, J.L., Fournier, R.A., Cote, J.F., Verstraete, M.M., 2011. Estimating leaf area distribution in savanna trees from terrestrial LiDAR measurements. Agric. For. Meteorol. 151, 1252–1266. https://doi.org/10.1016/j.agrformet.2011.05.004

Cifuentes, R., Van der Zande, D., Farifteh, J., Salas, C., Coppin, P., 2014. Effects of voxel size and sampling setup on the estimation of forest canopy gap fraction from terrestrial laser scanning data. Agric. For. Meteorol. 194, 230–240. https://doi.org/10.1016/j.agrformet.2014.04.013

Côté, J.F., Fournier, R.A., Egli, R., 2011. An architectural model of trees to estimate forest structural attributes using terrestrial LiDAR. Environ. Model. Softw. 26, 761–777. https://doi.org/10.1016/j.envsoft.2010.12.008

Durrieu, S., Allouis, T., Fournier, R., Véga, C., Albrech, L., 2008. Spatial quantification of vegetation density from terrestrial laser scanner data for characterization of 3D forest structure at plot level, in: SilviLaser 2008. pp. 325–334.

Gollob, C., Ritter, T., Wassermann, C., Nothdurft, A., 2019. Influence of scanner position and plot size on the accuracy of tree detection and diameter estimation using terrestrial laser scanning on forest inventory plots. Remote Sens. 11, 1–30. https://doi.org/10.3390/rs11131602

Grau, E., Durrieu, S., Fournier, R., Gastellu-etchegorry, J., Yin, T., 2017. Estimation of 3D vegetation density with Terrestrial Laser Scanning data using voxels . A sensitivity analysis of influencing parameters. Remote Sens. Environ. 191, 373–388. https://doi.org/10.1016/j.rse.2017.01.032

Hosoi, F., Nakai, Y., Omasa, K., 2010. Estimation and error analysis of woody canopy leaf area density profiles using 3-d airborne and ground-based scanning lidar remote-sensing techniques. IEEE Trans. Geosci. Remote Sens. 48, 2215–2223. https://doi.org/10.1109/TGRS.2009.2038372

Hosoi, F., Omasa, K., 2006. Voxel-based 3-D modeling of individual trees for estimating leaf area density using high-resolution portable scanning lidar. IEEE Trans. Geosci. Remote Sens. 44, 3610–3618. https://doi.org/10.1109/TGRS.2006.881743

Hu, R., Bournez, E., Cheng, S., Jiang, H., Nerry, F., Landes, T., Saudreau, M., Kastendeuch, P., Najjar, G., Colin, J., Yan, G., 2018. Estimating the leaf area of an individual tree in urban areas using terrestrial laser scanner and path length distribution model. ISPRS J. Photogramm. Remote Sens. 144, 357–368. https://doi.org/10.1016/j.isprsjprs.2018.07.015

Huang, P., Pretzsch, H., 2010. Using terrestrial laser scanner for estimating leaf areas of individual trees in a conifer forest. Trees - Struct. Funct. 24, 609–619. https://doi.org/10.1007/s00468-010-0431-z

Kamoske, A.G., Dahlin, K.M., Stark, S.C., Serbin, S.P., 2019. Leaf area density from airborne LiDAR: Comparing sensors and resolutions in a temperate broadleaf forest ecosystem. For. Ecol. Manage. 433, 364–375.

https://doi.org/https://doi.org/10.1016/j.foreco.2018.11.017

Li, Y., Guo, Q., Tao, S., Zheng, G., Zhao, K., Xue, B., Su, Y., 2016. Derivation, Validation, and Sensitivity Analysis of Terrestrial Laser Scanning-Based Leaf Area Index. Can. J. Remote Sens. 42, 719–729. https://doi.org/10.1080/07038992.2016.1220829

Morsdorf, F., Kükenbrink, D., Schneider, F.D., Abegg, M., Schaepman, M.E., 2018. Close-range laser scanning in forests: Towards physically based semantics across scales. Interface Focus 8. https://doi.org/10.1098/rsfs.2017.0046

Norman, J.M., Campbell, G.S., 1989. Canopy structure, in: Pearcy, R.W., Ehleringer, J.R., Mooney, H.A., Rundel, P.W. (Eds.), Plant Physiological Ecology: Field Methods and Instrumentation. Springer Netherlands, Dordrecht, pp. 301–325. https://doi.org/10.1007/978-94-009-2221-1_14

Pimont, F., Allard, D., Soma, M., Dupuy, J.-L.J.-L., 2018. Estimators and confidence intervals for plant area density at voxel scale with T-LiDAR. Remote Sens. Environ. 215, 343–370. https://doi.org/10.1016/j.rse.2018.06.024

Pimont, F., Dupuy, J.L., Caraglio, Y., Morvan, D., 2009. Effect of vegetation heterogeneity on radiative transfer in forest fires. Int. J. Wildl. Fire 18, 536–553. https://doi.org/10.1071/WF07115

Pimont, F., Soma, M., Dupuy, J.-L., 2019. Accounting for Wood, Foliage Properties, and Laser Effective Footprint in Estimations of Leaf Area Density from Multiview-LiDAR Data. Remote Sens. 11, 1580. https://doi.org/10.3390/rs11131580

Pimont, F., Soma, M., Dupuy, J.-L., Rigolot, E., Jean, F., 2016. Estimating canopy load and bulk density distribution using calibrated T-LiDAR indices, in: Proceedings for the 5th International Fire Behavior and Fuels Conference. International Association of Wildland Fire, Missoula, Montana, USA, Portland, Oregon, USA, pp. 3–8.

Ruel, J.J., Ayres, M.P., 1999. Jensen ' s inequality predicts effects of environmental variation.

Tree 5347, 361–366. https://doi.org/10.1016/S0169-5347(99)01664-X

Schlather, M., Malinowski, A., Menck, P.J., Oesting, M., Strokorb, K., 2015. Analysis, Simulation and Prediction of Multivariate Random Fields with Package RandomFields. J. Stat. Softw. 63. https://doi.org/10.18637/jss.v063.i08

Schneider, F.D., Kükenbrink, D., Schaepman, M.E., Schimel, D.S., Morsdorf, F., 2019. Quantifying 3D structure and occlusion in dense tropical and temperate forests using close-range LiDAR. Agric. For. Meteorol. 268, 249–257. https://doi.org/10.1016/j.agrformet.2019.01.033

Simioni, G., Marie, G., Huc, R., 2016. Influence of vegetation spatial structure on growth and water fluxes of a mixed forest: Results from the NOTG 3D model. Ecol. Modell. 328, 119–135. https://doi.org/10.1016/j.ecolmodel.2016.02.004

Soma, M., Pimont, F., Allard, D., Fournier, R., Dupuy, J.-L., 2020. Mitigating occlusion effects in Leaf Area Density estimates from Terrestrial LiDAR through a specific kriging method. Remote Sens. Environ. 245, 111836. https://doi.org/10.1016/j.rse.2020.111836

Soma, M., Pimont, F., Durrieu, S., Dupuy, J.-L.J.-L., 2018. Enhanced Measurements of Leaf Area Density with T-LiDAR: Evaluating and Calibrating the Effects of Vegetation Heterogeneity and Scanner Properties. Remote Sens. 10, 1580. https://doi.org/10.3390/rs10101580

Stark, S.C., Leitold, V., Wu, J.L., Hunter, M.O., de Castilho, C. V, Costa, F.R.C., McMahon, S.M., Parker, G.G., Shimabukuro, M.T., Lefsky, M.A., Keller, M., Alves, L.F., Schietti, J., Shimabukuro, Y.E., Brandão, D.O., Woodcock, T.K., Higuchi, N., de Camargo, P.B., de Oliveira, R.C., Saleska, S.R., 2012. Amazon forest carbon dynamics predicted by profiles of canopy leaf area and light environment. Ecol. Lett. 15, 1406–1414. https://doi.org/10.1111/j.1461-0248.2012.01864.x

Wang, D., Momo Takoudjou, S., Casella, E., 2020. LeWoS: A universal leaf-wood classification method to facilitate the 3D modelling of large tropical trees using terrestrial LiDAR. Methods Ecol. Evol. 11, 376–389. https://doi.org/10.1111/2041-210X.13342

Weiss, M., Baret, F., Smith, G.J., Jonckheere, I., Coppin, P., 2004. Review of methods for in situ leaf area index (LAI) determination Part II. Estimation of LAI, errors and sampling. Agric. For. Meteorol. 121, 37–53. https://doi.org/10.1016/j.agrformet.2003.08.001

Wilkes, P., Lau, A., Disney, M., Calders, K., Burt, A., Gonzalez de Tanago, J., Bartholomeus, H., Brede, B., Herold, M., 2017. Data acquisition considerations for Terrestrial Laser Scanning of forest plots. Remote Sens. Environ. 196, 140–153. https://doi.org/10.1016/j.rse.2017.04.030

Yan, G., Hu, R., Luo, J., Weiss, M., Jiang, H., Mu, X., Xie, D., Zhang, W., 2019. Review of indirect optical measurements of leaf area index: Recent advances, challenges, and perspectives. Agric. For. Meteorol. 265, 390–411. https://doi.org/10.1016/j.agrformet.2018.11.033

Yun, T., Cao, L., An, F., Chen, B., Xue, L., Li, W., Pincebourde, S., Smith, M.J., Eichhorn, M.P., 2019. Simulation of multi-platform LiDAR for assessing total leaf area in tree crowns. Agric. For. Meteorol. 276–277, 107610. https://doi.org/10.1016/j.agrformet.2019.06.009

Zhao, K., García, M., Liu, S., Guo, Q., Chen, G., Zhang, X., Zhou, Y., Meng, X., 2015. Terrestrial lidar remote sensing of forests: Maximum likelihood estimates of canopy profile, leaf area index, and leaf angle distribution. Agric. For. Meteorol. 209–210, 100–113. https://doi.org/10.1016/j.agrformet.2015.03.008

Appendix A

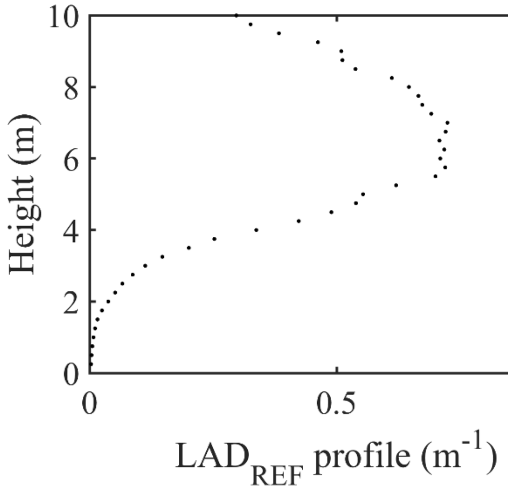

A1. Vertical profile of simulated reference Leaf Area Density 3D field.

Appendix B

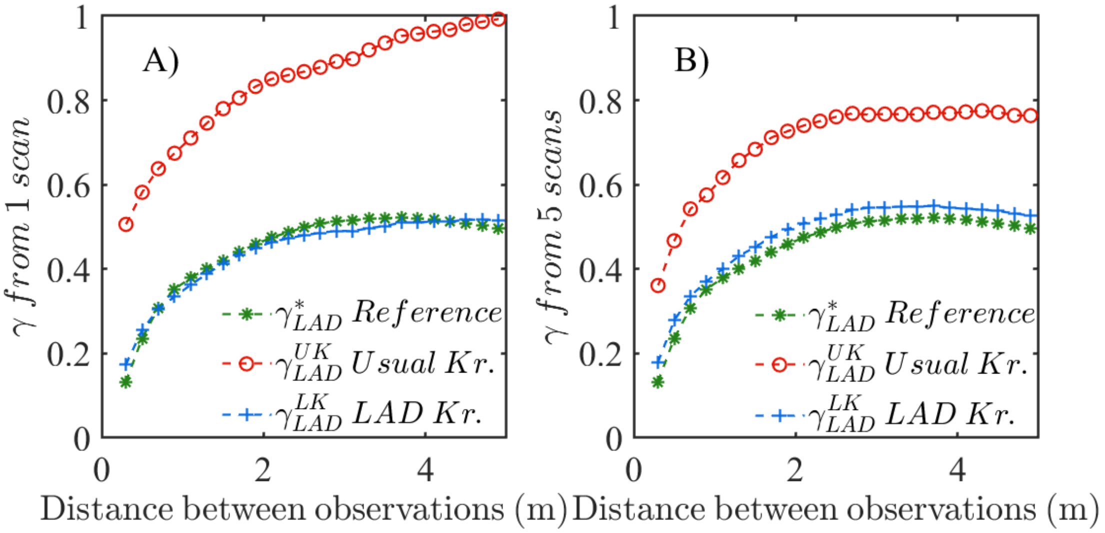

B1. Variogram of the reference vegetation scene (green crosses). Estimated variograms from $\widetilde{LAD}$ computed for usual kriging method (red circle) and with the kriging method specific to LAD (blue cross) for the scan design corresponding to A) Single viewpoint; B) Five viewpoints. For more details, please refers to Soma et al. 2020.

Appendix C

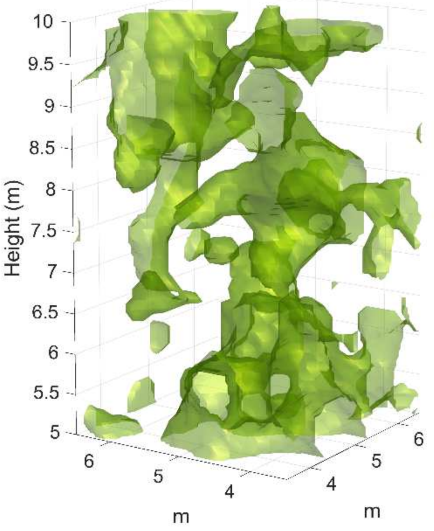

C1. Isosurface of the simulated vegetation scene from RandomFields package. To ease visualization, only a subsample of the scene is displayed (core of the plot).

Appendix D

We assessed the significance of voxel size and number on scans effects on estimations though a statistical analysis. Voxels resulting from the fine and coarse discretization levels of the vegetation scene cannot be considered as independent observations when comparing voxel sizes, as voxels share the same vegetation in occupied volumes, with respect to their size (e.g. several 0.1 m voxels are contained in the 0.5 m voxel at the same location). To account for such specificity, all estimations were smoothed to the largest voxel size voxels, i.e. 1 m, and tests were performed at this scale. Smoothing was done by averaging 0.1 m – 0.2 m and 0.5 m voxels with respects to the 1 m voxel size grid. As voxels arise from the same vegetation scene, observations (voxels) cannot be considered independent between treatments (voxel size * number of scans), but should be considered as a repeated measure on the same individual. Hence, we performed a two-way ANOVA with repeated measures using R software (R Core Team (2016). R: A language and environment for statistical computing. R Foundation for Statistical Computing, Vienna, Austria. URL https://www.R-project.org/). The analysis was carried out with estimation errors $(LAD_{REF,i} - \widetilde{LAD}_i)$ as predictor, for the 0.1 m, 0.2 m, 0.5 m and 1 m voxel sizes and for the two scans and five scans designs :

$$(LAD_{REF,i} - \widetilde{LAD}_i) \sim IDvox/\ (Voxel\ size + Number\ of\ scans)$$

with *IDvox* the voxel ID used for the within-subject model computation.

Effects	**D.F.**	**F-value**	**P-Value**
IDvox	999	-	-
IDvox : Voxel size	3	27.1	2e-16 ***
IDvox : Number of scans	1	34.31	6.4e-9 ***

In accordance with graphical observations, both effects of voxel size and of number of scans are significant on the error in estimation of LAD value.